

Electrochemical preparation of oligo(azulene) on nanoporous TiO₂ and characterization of the composite layer

Rose-Marie Latonen · Carita Kvarnström · Ari Ivaska

Received: 22 June 2009 / Accepted: 18 April 2010 / Published online: 29 April 2010
© Springer Science+Business Media B.V. 2010

Abstract A nanoporous oligo(azulene)-TiO₂ (OAz-TiO₂) composite layer was formed by electrochemical oxidation of azulene (Az) on a nanoporous ITO/TiO₂ electrode. Polymerization was performed in tetrabutylammonium hexafluorophosphate electrolyte salt dissolved in acetonitrile. The electrochemical and optical properties of the composite layer were studied by cyclic voltammetry (CV) and in situ UV-vis spectroelectrochemistry. The chemical and crystalline structure of the layer was studied by FTIR and X-ray diffraction (XRD) spectroscopy techniques and the morphology by Scanning Electron Microscopy. The TiO₂ layer was found to have a catalytic activity on the polymerization of Az. The CV experiments in monomer-free electrolyte solution demonstrated the electron donor property of OAz by its p-doping and the electron accepting property of TiO₂ by the large reduction current in the negative potential region. The FTIR and XRD spectroscopic measurements showed the well-defined anatase structure of TiO₂ with inclusion of OAz. A composite layer was formed rather than a bilayer structure. The in situ UV-vis spectroelectrochemical measurements gave evidence of a higher delocalization and easier movement of the π -electrons in the composite layer than in pure poly(azulene).

Keywords Oligo(azulene) · TiO₂ · Electropolymerization · Composite · Solar cell

1 Introduction

There is a great activity in making devices based on nanostructure architectures for solar energy conversion. In this field of research inorganic semiconductors like TiO₂, ZnO, and SnO₂ combined with different organic molecules or polymers, metal nanoparticles or combinations of these have gained much interest [1–3]. Organic semiconducting materials such as electrically conducting polymers (ECPs) combined with the inorganic semiconductor TiO₂ with a band gap of 3.2 eV (anatase crystallographic form) have attracted considerable attention in solar cell applications [4–17]. ECPs are used as dyes which sensitize TiO₂ to visible radiation. The most successful sensitizers for solar cell applications are ruthenium polypyridyl complexes anchored to nanocrystalline TiO₂ in the concept of the Grätzel cell [18]. There are, however, some drawbacks like evaporation of the electrolyte, stability of the electrolyte and the dye, as well as the high cost and the limited availability of the dye [5]. The high ability to absorb light in the visible part of the spectrum, the high mobility of the charge carriers in ECPs as well as their low cost, easy availability and flexibility make them good candidates as sensitizers to be used in solar cell applications [4–10, 13].

The diffusion length of excitons in ECPs is typically 5–15 nm. It has been shown that most of the photogenerated excitons which lead to charge separation occur at the interface between the polymer and the nanocrystals [12]. Therefore, to prevent unwanted recombination of the formed excitons a large interface area between the

R.-M. Latonen (✉) · A. Ivaska
Process Chemistry Centre, c/o Laboratory of Analytical Chemistry, Åbo Akademi University, Biskopsgatan 8, 20500 Turku, Finland
e-mail: rlatonen@abo.fi
URL: <http://web.abo.fi/fak/tkf/ank>

C. Kvarnström
Laboratory of Materials Chemistry and Chemical Analysis, Department of Chemistry, University of Turku, Vatselankatu 2, 20014 Turku, Finland

acceptor-type TiO_2 and the donor-type ECP is needed. Also the ratio of donor and acceptor in TiO_2 -ECP devices is critical for successful charge separation. Charge recombination is suppressed by having only a thin polymer layer attached to TiO_2 . Furthermore, most of the produced charge originates from charge separation events occurring at the first nanocrystal layers closest to the electrode surface [12]. Different ways to synthesize a nanoporous ECP- TiO_2 composite have been used: self-assembly on nanoporous TiO_2 by carboxylic acid groups in the sensitizing ECP [4–7], surface modification of TiO_2 followed by chemical polymerization of the ECP [8], spin-coating or dip-coating of soluble ECP [9–12], sol-gel reaction [13, 14] and electropolymerization of the ECP on nanoporous TiO_2 [15, 16]. In this study an oligo(azulene)- TiO_2 (OAz- TiO_2) composite layer has been formed by electrochemical polymerization of azulene (Az) on a nanoporous ITO/ TiO_2 electrode. The interface area between the OAz phase and the TiO_2 phase is expected to increase by using the electropolymerization technique. This is due to the higher accessibility of a monomer to the small pores in the TiO_2 layer compared to that of a polymer chain. An OAz layer rather than a poly(azulene) (PAz) layer is therefore expected to be formed in the pores. The polymer layer thickness is also easy to control by the electropolymerization technique and formation of thin polymer layers is therefore possible. Moreover, a soluble polymer is not required and monomers without any solubilizing side chains can be used. The structure of PAz is based on fused-rings, which is expected to have a reducing effect on the band gap [19, 20]. In order to cover most of the solar spectrum, ECPs with an appropriately low band gap are highly sought [20]. The absorbance of PAz in the UV and visible spectral regions is also rather broad [20–26] making PAz an attractive material for applications in solar cells. PAz has also been shown to have electron-donating properties [21, 28–32]. The oxidized form of the fused-ring monomer Az, resonance-stabilized azulenylium carbocation, used in this study is very stable [33]. It has been reported that 1-carboxyazulene in its excited state can inject an electron into the conduction band of TiO_2 within the fs time scale [33, 34]. Furthermore, the easy electropolymerization process of Az [20–25, 28, 34–36], having a relatively low oxidation potential, makes PAz a good candidate as an electron donor material combined with TiO_2 . The nanoporous OAz- TiO_2 composite material studied in this study has been characterized by cyclic voltammetry (CV), in situ UV-vis spectroelectrochemistry, FTIR spectroscopy, X-ray diffraction (XRD) spectroscopy, and Scanning Electron Microscopy (SEM).

2 Experimental

Formation of the studied nanoporous OAz- TiO_2 composite layer and the charging-discharging experiments were carried out in a conventional three-electrode one-compartment electrochemical cell. The cell was connected to an Autolab PGSTAT100 potentiostat using General Purpose Electrochemical System software. The working electrode was an optically transparent indium tin oxide (ITO) glass (Delta Technologies, Limited, 4–8 Ω square $^{-1}$) covered with a transparent nanoporous TiO_2 layer (ITO/ TiO_2 electrode). The ITO electrodes were cleaned with chloroform and with acetone during 30 min in an ultrasonic bath before applying the TiO_2 paste on top of them. The nanoporous TiO_2 layer was prepared by the doctor-blade (squeegee) printing method of nanocrystalline TiO_2 paste (Solaronix Ti-Nanoxide T/SP, 13 nm \varnothing anatase particles, $\sim 120 \text{ m}^2 \text{ g}^{-1}$ surface area). Two pieces of Scotch Magic tape (3 M) were adhered on both edges of the ITO electrode. An amount of approximately 10 $\mu\text{L cm}^{-2}$ of the TiO_2 paste was then spread out evenly between the two adhesive tapes on the surface of the ITO electrode by use of a microscope slide. After letting the TiO_2 paste to dry for about 35 min the adhesive tapes were removed and the electrodes were placed in an oven with a temperature of approximately 70 °C. Temperature was then slowly increased to 450 °C, and the material was then sintered for 30 min at this temperature in air. By this procedure a 6–8 μm thick nanoporous TiO_2 layer (measured by SEM) with a particle size of 30–40 nm was formed. A Pt wire was used as the counter electrode. All potential values were measured against a Ag wire covered with AgCl as a pseudo reference electrode (calibrated against ferrocene/ferrocenium, $E_{\text{redox}} = 0.36 \text{ V}$ in 0.1 M TBAPF₆-ACN). OAz was polymerized by potential cycling between –0.6 and 1.2 V with a scan rate of 50 mV s $^{-1}$ in 0.1 M tetrabutylammonium hexafluorophosphate (TBAPF₆, Fluka) electrolyte salt in acetonitrile (ACN, Lab-Scan). The ITO/ TiO_2 substrates were always immersed in the polymerization/electrolyte solution so that the electrochemically active area was kept approximately the same. After polymerization the formed nanoporous OAz- TiO_2 composite layers were let to relax and stabilize in pure ACN for approximately 30 min before drying and further characterization. If this step was ignored the TiO_2 -OAz composite layer cracked and came easily off from the electrode surface. ACN was freshly distilled and dried over basic alumina (~ 150 mesh, Aldrich) just before it was used and stored over CaH₂. The electrolyte salt TBAPF₆ was dried at 80 °C under vacuum for 1 h. Concentration of the monomer azulene (Az, Aldrich) was 10 mM, and it was used as received. All solutions were deaerated with nitrogen prior to

measurements, and all the measurements were done under nitrogen atmosphere.

The ex situ FTIR reflection measurements of the nanoporous OAz-TiO₂ composite layers on ITO glass substrates were performed using a Seagull™ variable angle reflectance accessory (Harric Scientific) with an angle of incidence of 45°, and 500 interferograms were recorded for each spectrum. The resolution used was 4 cm⁻¹. The spectra were recorded on a Bruker IFS 66/S FTIR instrument equipped with an MCT detector.

For the in situ UV-vis spectroscopic experiments OAz was deposited on the nanoporous ITO/TiO₂ electrodes in the same way as for the electrochemical measurements. The path length of the quartz cuvette used was 1 cm. The reference electrode was the same as in the CV experiments, and a Pt wire was used as the counter electrode. The potential was held at a constant value for 80 s before each measurement and increased then by steps of 200 mV in the beginning of the positive potential scan and by steps of 100 mV at the potential range where the Faradaic process occurs. The spectra were recorded between 340 and 1100 nm on a Hitachi U-2001 spectrophotometer.

For XRD analysis OAz was deposited on nanoporous ITO/TiO₂ electrodes in the same way as described earlier. The nanoporous OAz-TiO₂ composite layers were dried and used directly for X-ray diffractional analysis without any further processing. The diffractograms were recorded on a conventional X-ray scanning diffractometer, Phillips PW3710BASED, using Cu K α radiation with the wavelength of 1.54 Å. A Zeiss, Leo 1530 Gemini Scanning Electron Microscope with a ThermoNoran, Vantage X-ray detector was used to obtain the SEM micrographs.

3 Results and discussion

3.1 Polymerization and cyclic voltammetric characterization of the nanoporous OAz-TiO₂ composite layer

The CV responses of nanoporous ITO/TiO₂ (solid line) and bare ITO (dashed line) electrodes in 0.1 M TBAPF₆-ACN electrolyte solution in two different potential regions are shown in Fig. 1. The CV response of the ITO/TiO₂ electrode in the potential region between -0.6 and 1.2 V shows that oxidation of the nanoporous TiO₂ layer starts approximately at 0.8 V and reduction approximately at -0.4 V. The small oxidation peak at around 0 V can be assigned to Ti³⁺ species formed by electrochemical reduction of the fresh TiO₂ surface [37]. That peak was not observed when the potential was scanned to less negative potentials, i.e., -0.2 V. The newly created Ti³⁺ is very reactive and the peak disappears after successive potential

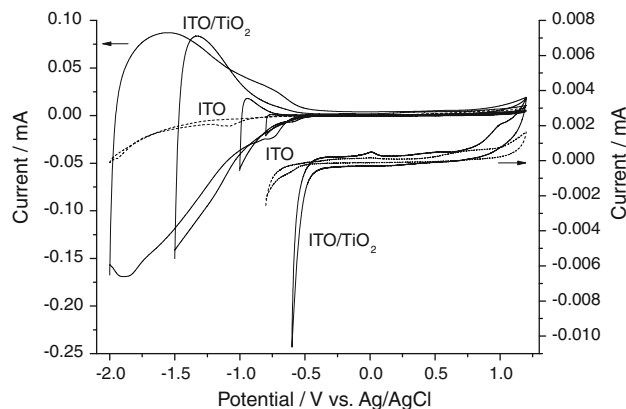


Fig. 1 The cyclic voltammograms of bare nanoporous ITO/TiO₂ (solid line) and ITO (dashed line) electrodes in 0.1 M TBAPF₆-ACN electrolyte solution, scan rate 50 mV s⁻¹. Observe two different current scales

scanning. By scanning the potential more negative than -0.6 V the cathodic current increases steadily and after the potential is scanned to -0.8 V and even to more negative potentials a distinguished anodic peak is observed on the reverse scan. The reversible large reduction current obtained from the ITO/TiO₂ electrode at potentials more negative than -0.6 V demonstrate the electron accepting property of TiO₂. The rather symmetric shape of the CVs indicates the capacitive nature of the film charging and an effective movement of charge throughout the whole film. An additional pair of redox peaks is located between -0.5 and -0.8 V and can clearly be seen on the CV scanned to -2.0 V. These peaks have been found to be characteristic for nanostructured electrodes and assigned to reversible filling of surface states below the conduction band edge, which confirms presence of electron trap states [38–42]. The density of these electron traps at surface sites is strongly dependent on the morphology of the electrode.

A continuous growth of the polymer film on ITO/TiO₂ electrode was observed during potential cycling in monomer solution. However, with this experimental setup five potential cycles (103.2 mC) were found to be the maximum number of cycles during polymerization that resulted in formation of a mechanically stable nanoporous OAz-TiO₂ composite layer after letting the electrode to relax in pure ACN. Continuous cycling (after five cycles) in monomer solution resulted in further film growth, but after letting the formed composite layer to dry it cracked and came off from the electrode surface. The potentiodynamic polymerization of 10 mM Az in 0.1 M TBAPF₆-ACN between -0.6 and 1.2 V with a scan rate of 50 mV s⁻¹ on ITO/TiO₂ electrode is shown in Fig. 2a. For comparison the five first potential cycles during polymerization of 10 mM Az in the same electrolyte solution but on bare ITO electrode are shown in Fig. 2b. Potential cycling of ITO/

TiO_2 in 0.1 M TBAPF₆-ACN without the monomer did not show any current in the potential region between −0.4 and 0.1 V where TiO_2 is non-conducting. No current could either be recorded in the same potential region when Az was polymerized on pure ITO (see Fig. 2b). The current between −0.6 and 0.1 V during polymerization of Az on ITO/TiO₂ (Fig. 2a) became visible only after OAz formation was initiated by the first potential scan to 1.2 V. TiO_2 may be reduced and starts to accept electrons from the oxidation products of Az monomers at potentials below 0.1 V. The growing current response in that potential region may, therefore, originate from the reduction and reoxidation of the TiO_2 layer in the OAz-TiO₂ composite during polymerization of Az.

The first cycles during polymerization of 10 mM Az on ITO (dashed line) and on ITO/TiO₂ (solid line) electrodes in 0.1 M TBAPF₆-ACN are shown in Fig. 3. It can be observed that oxidation of Az starts at approximately 0.25 V lower potential on ITO/TiO₂ electrode than on ITO electrode. Lowering the onset potential of Az oxidation

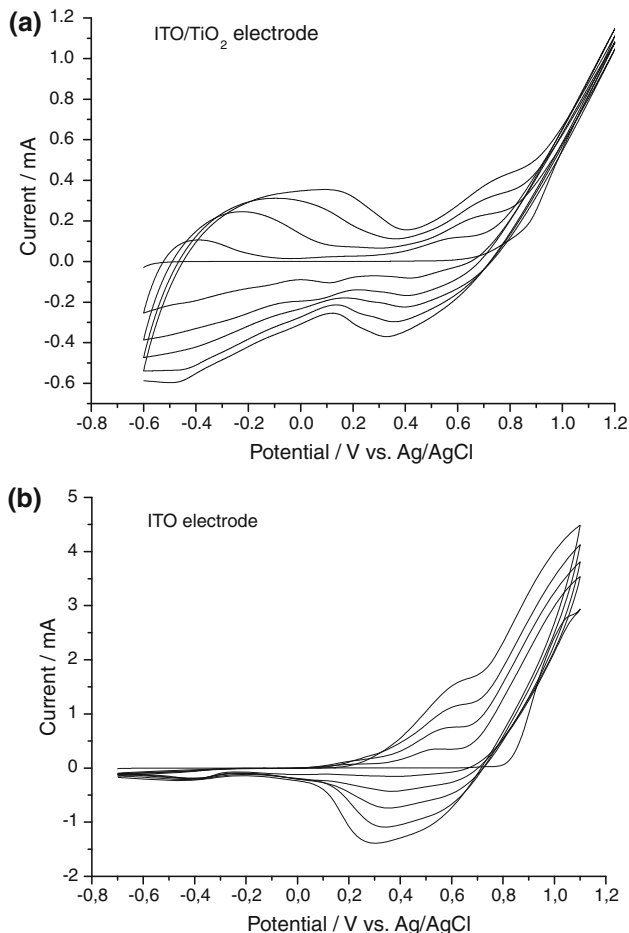


Fig. 2 Cyclic voltammograms during polymerization of 10 mM Az in 0.1 M TBAPF₆-ACN between −0.6 and 1.2 V (a) on ITO/TiO₂ electrode and (b) on bare ITO electrode. Scan rate 50 mV s^{−1}

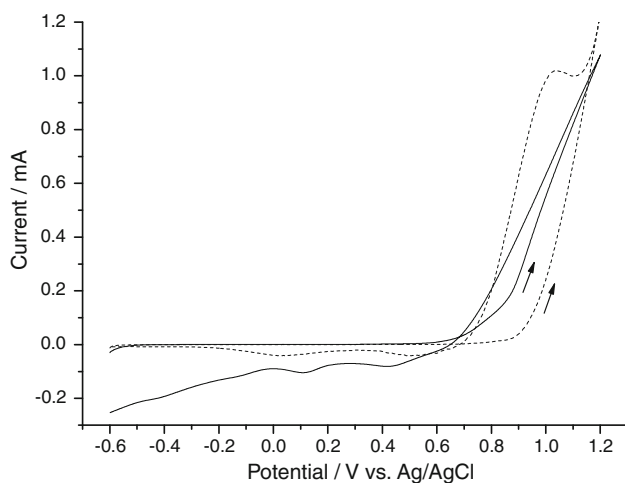


Fig. 3 The first cycles during polymerization of 10 mM Az on ITO (dashed line) and on ITO/TiO₂ (solid line) electrodes in 0.1 M TBAPF₆-ACN electrolyte solution, scan rate 50 mV s^{−1}

demonstrates the catalytic activity of TiO_2 toward polymerization of Az. This may be due to the electron withdrawing effect of TiO_2 that accelerates oxidation of the monomer. The same kind of catalytic activity of TiO_2 has also been observed in electropolymerization of pyrrole [43] and Az [44] in solutions containing TiO_2 nanoparticles.

The charging–discharging reaction of the nanoporous OAz-TiO₂ composite layer made as in Fig. 2a was studied in monomer-free electrolyte solution. The CV response is strongly dependent on the potential interval used. Fig. 4a shows the CVs of OAz-TiO₂ composite layer when potential cycling was performed to 0.6, 0.9, and 1.0 V starting from −0.4 V. In each CV the third cycle in the respective potential region is shown. p-doping of OAz in the nanoporous TiO_2 layer starting at approximately 0 V in the positive potential scan demonstrates the electron donor property of OAz [21, 28–32]. The current response in the capacitive charging region of OAz-TiO₂ composite layer between −0.4 and 0.35 V depends strongly on the degree of the remaining charge in OAz after oxidation. When performing potential scanning between −0.4 and 0.95 V, OAz gives rise to charging of the interface between the donor-type OAz and the acceptor-type TiO_2 . This kind of a charging current cannot be observed in a pure PAz film on ITO. Figure 4b shows the evolution of CV responses during potential cycling of the same composite layer as in Fig. 4a to the negative potential region. Again the third cycle in each CV in the respective potential region is shown. A prepeak in the positive potential scan can be observed in the potential region between 0.1 and 0.4 V. The magnitude of this prepeak and the reduction of it during reversed potential scan is dependent on how far in the negative region the potential is scanned (see Fig. 4b). By performing a more intense reduction of the

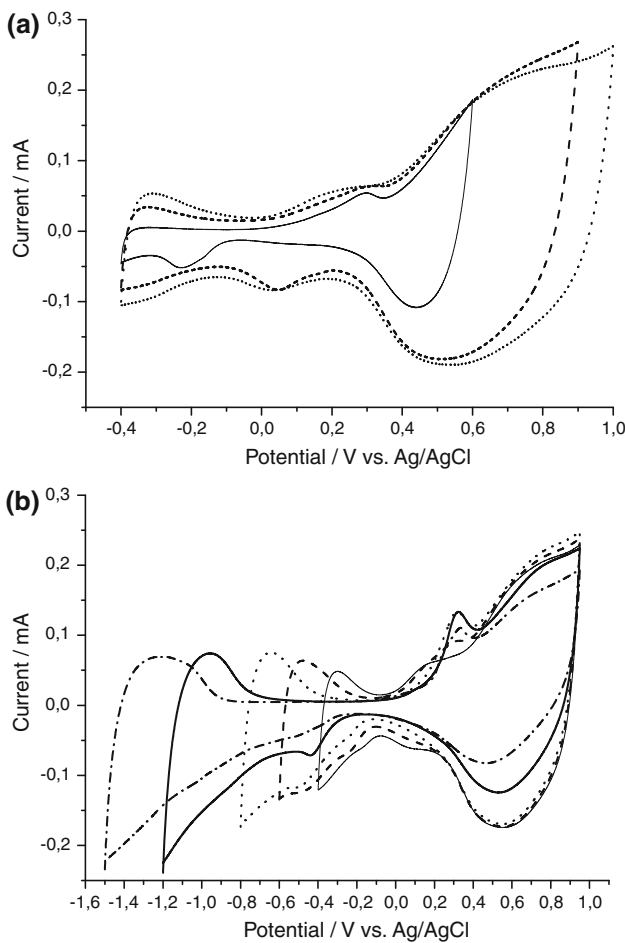


Fig. 4 The cyclic voltammetric responses of the OAz-TiO₂ composite layer made as in Fig. 2a, (a) from −0.4 V by successively increasing potentials until 1.0 V and (b) by successively decreasing negative potentials starting from −1.5 V in 0.1 M TBAPF₆-ACN electrolyte solution, scan rate 20 mV s^{−1}

TiO₂ layer the above-mentioned redox process seems also to become more irreversible. The origin of the redox reaction can be assigned to trapped conduction carriers, a phenomenon called charge trapping [45–49]. During *n*-doping process, OAz is partially reduced and negative charge carriers are formed with subsequent insertion of TBA⁺ from the electrolyte solution. Upon reversal of the potential scan only a portion of OAz will be neutralized due to its low electrical conductivity. Hence, some negative charge carriers are left isolated and are trapped in the composite layer. When a critical number of positive charge carriers are formed during *p*-doping they can interact with the trapped negative charge carriers and cause the prepeak seen in the CV. This kind of a phenomenon is also observed clearly in a fullerene-PAz composite [50]. Furthermore, the current observed between −0.4 and 0.35 V decreases successively by increasing the negative vertex potential of cycling. Obviously, an irreversible change in the structure of OAz occurs when the composite layer is

cycled to potentials more negative than −0.8 V. This change may cause the decrease in the current within the capacitive current region between −0.4 and 0.35 V. The onset potential for reduction of the OAz-TiO₂ layer starts between −0.1 and −0.25 V depending on the negative start potential of the potential scanning. Reduction of pure ITO/TiO₂ layer, however, is observed to start at −0.4 V (see Fig. 1). This means that reduction and subsequent oxidation of TiO₂ is easier in the OAz-TiO₂ composite layer than in pure TiO₂ and the electron accepting power of TiO₂ is enhanced in the composite.

Stability measurements of the OAz-TiO₂ composite layers using CV in monomer-free electrolyte solution were performed in two different potential regions, −0.4-(+0.9) V and −1.9-(+0.9) V. Fig. 5a shows the CV response of 140 successive cycles in 0.1 M TBAPF₆-ACN using 20 mV s^{−1} scan rate in the potential region −0.4-(+0.9) V. It can be observed that the current response from the redox process occurring in the potential region between 0 and

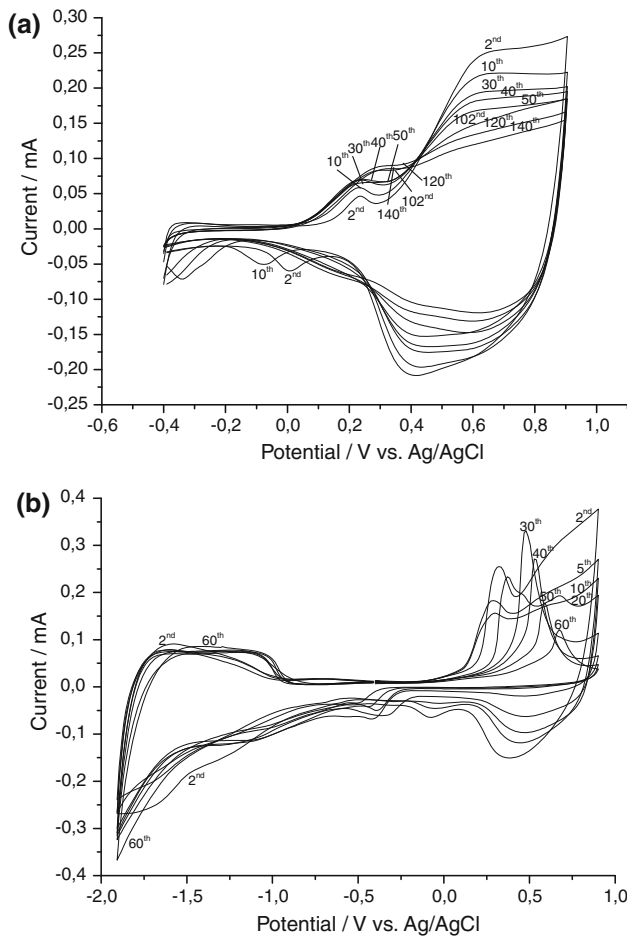


Fig. 5 The cyclic voltammetric response of OAz-TiO₂ composite layer after (a) 140 cycles between −0.4 and 0.9 V and (b) 60 cycles between −1.9 and 0.9 V in 0.1 M TBAPF₆-ACN electrolyte solution, scan rate 20 mV s^{−1}

0.4 V increases and the current response from the redox process occurring in the potential region between 0.4 and 0.9 V decreases by successive potential cycling. The reason for this could be that partly reduced TiO_2 accepts electrons from the oxidized OAz and reoxidation of it becomes easier after multiple potential cycling. The total charge involved in the redox reaction diminishes during 140 potential cycles (cycle 2: $12.4 \times 10^{-3} \text{ C}$, cycle 50: $10.2 \times 10^{-3} \text{ C}$, cycle 102: $9.7 \times 10^{-3} \text{ C}$, cycle 140: $8.3 \times 10^{-3} \text{ C}$). Figure 5b shows the CV response during 60 cycles in the potential region -1.9 – $(+0.9)$ V. In that potential region the current response for reduction and reoxidation of TiO_2 in the composite layer is relatively reproducible during multiple potential cycling. The current response for oxidation and rereduction of OAz in the composite layer, on the other hand, diminishes and becomes narrower. This phenomenon can be explained by an irreversible structural change of OAz during n-doping on ITO substrates [31].

3.2 Characterization by X-ray diffraction analysis

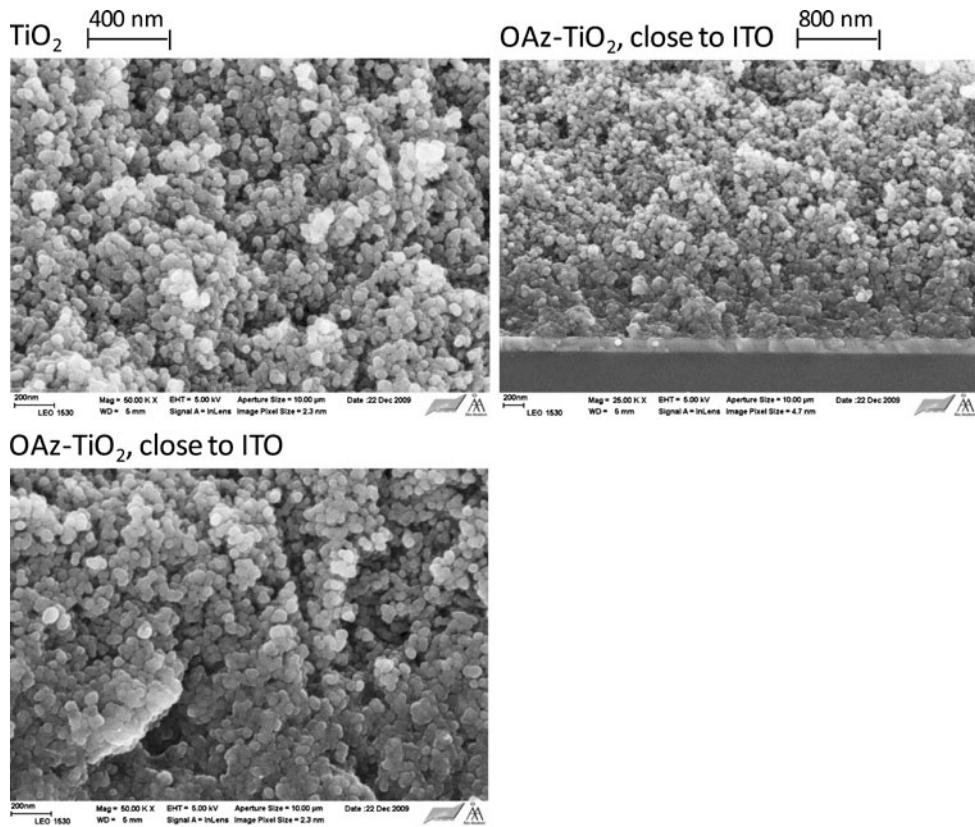
The XRD pattern for nanoporous TiO_2 shows formation of an anatase-like crystalline network structure having diffraction peaks at the angle of incidence to the sample plate (2θ) of 25.2° , 37.8° , 48.0° , and 53.9° [14, 51–53]. The

XRD peaks from the nanoporous TiO_2 layer are somewhat wider than the peaks from highly crystalline TiO_2 . This is an evidence for formation of a TiO_2 layer with induced porosity [14]. The diffractogram of the OAz- TiO_2 composite layer does not differ much from the diffractogram of the nanoporous TiO_2 layer. Only reduced intensity of the TiO_2 and ITO peaks was observed. Any XRD patterns assigned to the conducting polymer structure in poly(3,4-ethylenedioxythiophene)-poly(styrene sulfonate)/ TiO_2 composites [14] or polyaniline/ TiO_2 composite nanofibres [52] have not either been observed. These results also indicate that the electropolymerization of OAz did not change the structure of TiO_2 .

3.3 Scanning Electron Microscopy characterization

Morphology of the OAz- TiO_2 composite layer was also studied by SEM and compared with the morphology of the nanoporous TiO_2 layer. The SEM micrographs from the cross sections of the ITO/ TiO_2 electrode and the OAz- TiO_2 composite layer are shown in Fig. 6. The doctor-blade printing method of the nanocrystalline TiO_2 paste (13 nm \varnothing anatase particles) followed by sintering at 450 °C formed a rather homogeneous nanoporous morphology of TiO_2 with a layer thickness of 6–8 μm on the surface of the ITO substrate. Pore sizes seem to be <80 nm. Electropolymerization

Fig. 6 SEM micrographs from the cross sections of the ITO/ TiO_2 electrode and the ITO/OAz- TiO_2 composite layer with two magnifications



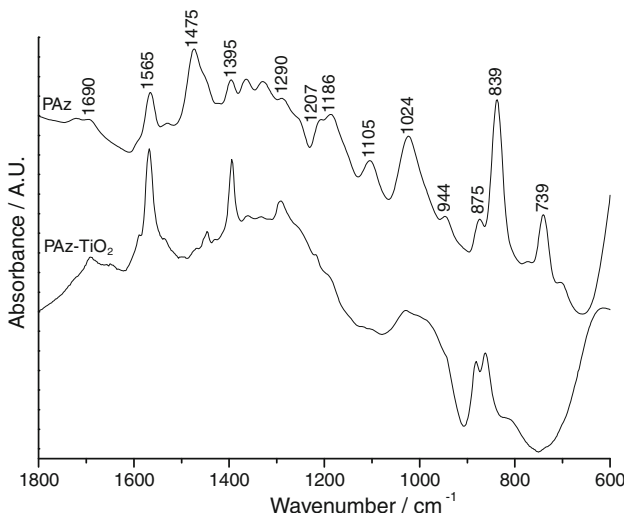


Fig. 7 The ex situ FTIR spectra of the nanoporous OAz-TiO₂ layer and of the PAz film using a spectrum of ITO/TiO₂ electrode and ITO, respectively, as reference

of 10 mM Az in 0.1 M TBAPF₆-ACN did not change the morphology of the nanoporous TiO₂ layer. Only a small difference in the roughness of the layer could be observed. These results also indicate that the OAz film was not formed as a uniform layer on top of the TiO₂ layer. This result is consistent with the XRD analysis results. It could rather be said that the OAz film filled the pores in the TiO₂ layer within approximately 0.8 μm from the ITO electrode surface. Based on the SEM micrographs, however, it is difficult to say if the OAz film was formed throughout the nanoporous structure of the TiO₂ layer. Also electropolymerization of poly(3-methylthiophene) in nanoporous TiO₂ matrix has been shown to begin from the bottom of the ITO electrode before the pores in the nanoporous structure of TiO₂ become uniformly filled with the growing polymer [15].

3.4 FTIR characterization

The ex situ reflection spectrum of the nanoporous OAz-TiO₂ composite layer in the electrically neutral state formed on top of ITO glass is shown in Fig. 7. It should, however, be pointed out that some parts of the film may be in conductive state due to no separate reduction step has been performed after synthesis. The reference spectrum used is from the ITO/TiO₂ electrode. The spectrum of the composite layer is compared with the spectrum of PAz film electrochemically polymerized on ITO glass electrode using 10 mM monomer dissolved in 0.1 M TBAPF₆-ACN electrolyte solution (see Fig. 7). The reference spectrum used in that case is from an ITO electrode. The peaks at 1565 cm⁻¹ [54, Table 11.1–56], at 1475 cm⁻¹ [54, Table 11.1], and at 1395 cm⁻¹ [26, 56] in both spectra are

assigned to aromatic C=C ring stretching vibrations. PAz [28] and the OAz-TiO₂ [44] composite layer show intense infrared active vibration bands in the wavenumber region around 1500 cm⁻¹. The intensity of the band at 1475 cm⁻¹ in the spectrum of PAz (almost invisible in the spectrum of OAz-TiO₂ composite) may indicate that PAz on ITO is in more conductive state than the composite layer. Az monomer has a band at 1395 cm⁻¹ [25] which is more intense in the spectrum of the composite layer than in PAz. This can be regarded as evidence of formation of shorter chains in the composite due to monosubstituted Az units. The =C-H ring out-of-plane deformation vibration can be seen as a strong band at 739 cm⁻¹ [25, 54, Table 11.2, 26, 55, Table 9.22, 56] and as a couple of weak bands at 875 and 944 cm⁻¹ [55, Table 9.22]. The vibrational bands in the wavenumber region 1020–1290 cm⁻¹ can be assigned to =C-H in-plane deformation vibrations [25, 54, Table 11.4]. The strong band at 839 cm⁻¹ in the spectrum of PAz is due to the vibration originating from the doping anion PF₆⁻ [54, Table 22.1]. The band from the doping anion in the spectrum of the composite may have a lower intensity than in the PAz spectrum and be located under the broader band between 830 and 900 cm⁻¹ which is assigned to a doping-induced band [28, 44].

3.5 In situ UV-visible spectroelectrochemical characterization

In the UV-visible spectroelectrochemical measurements the p-doping process of OAz in the nanoporous TiO₂ layer was studied by recording spectra at different potentials applied to the electrode. Before recording the spectra at each potential the potential was held at that value for 80 s in order to convert the material to the new electronic state. The polymer was synthesized by potential cycling in 10 mM Az in 0.1 M TBAPF₆-ACN solution either on the nanoporous ITO/TiO₂ electrode or on the ITO glass electrode. The in situ UV-vis spectra of stepwise doping of the OAz-TiO₂ layer and the PAz film are shown in Fig. 8a and b, respectively. In Fig. 8a a spectrum recorded from the nanoporous ITO/TiO₂ electrode has been used as the background. In the case of the PAz spectra a spectrum recorded from ITO has been used as the background. The nanoporous TiO₂ layer gives a weak absorption in the visible spectral region (shown in the inset of Fig. 8a). This is most probably due to scattering of light by the TiO₂ film. No changes were, however, observed in the spectrum of TiO₂ at different applied potentials. The valence to conduction band ($\pi-\pi^*$) transition, which is connected to the mean conjugation length of the chains and to delocalization of the π electrons [57], is seen in the spectrum of neutral OAz in the composite at 475 nm and in the spectrum of neutral PAz film at 412 nm. The absorption maximum of neutral PAz

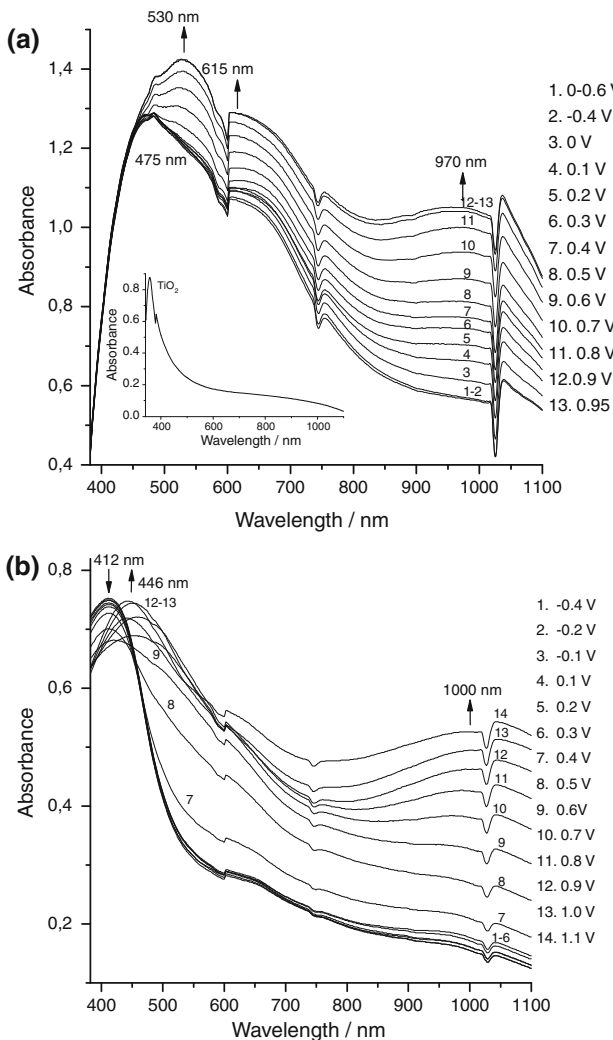


Fig. 8 The in situ UV-vis spectra of stepwise doping of (a) OAz-TiO₂ composite and (b) PAz film in 0.1 M TBAPF₆-ACN electrolyte solution. The inset in (a) shows the absorption spectrum of TiO₂

has also been reported by other groups [20–27] to be around 420 nm for both chemically and electrochemically synthesized PAz films. As the absorption maximum of OAz in the composite structure is located at 63 nm higher wavelength it can be concluded that delocalization of the π electrons in OAz in nanoporous TiO₂ is increased. The vicinity of electron accepting TiO₂ decreases the width of the energy gap and makes excitation of electrons to take place easier from the valence band of OAz to the conduction band. Film thickness has also an effect on the degree of conjugation and the macroscopic morphological order of the film. Usually a thinner film has its UV-vis absorbance maximum at longer wavelength compared to a thicker film. This is explained by a less ordered structure in a thick film. The OAz layer in the composite may be thinner than the PAz film on ITO which can also partly cause the shift of the absorbance maximum to higher wavelength.

Oligo(azulene) in the neutral state has both in the composite structure and also as a PAz film an additional absorption band located at around 615 nm. This band is due to absorption of Az monomer, which also causes its blue color, and is related to the small band gap of Az [20]. According to the method used by Daub et al. [20] the mean effective conjugation length of the OAz in the nanoporous TiO₂ layer can be estimated to 2.2 monomer units and the band gap $E_g = 2.0$ eV. This approximation is based on the linear correlation between the energy of the lowest absorption maximum and the inverse chain length of chemically synthesized oligomers of different length. This particular band, however, has a much lower intensity in the spectrum of the PAz film which may mean that in the OAz-TiO₂ composite some Az monomer is left. This kind of a broad absorbance in the UV-vis spectral region of the neutral state of PAz has also been reported earlier [20–26] and can be regarded as a benefit in further development of this kind of material for solar cell applications.

Electrochemical doping of OAz in the composite structure results in a continuous growth of two new absorption bands: at 530 nm and around 1000 nm. These bands grow continuously in intensity during increase of the applied potential. Growth of absorption bands at 526 nm and at around 1300 nm and at 590 nm and at around 1600 nm during stepwise doping of an electrochemically synthesized PAz film has also been reported by Nöll et al. [20], respectively, Österholm et al. [31]. The corresponding doping-induced absorption bands of the PAz film made in this study can be seen at 446 nm and at around 1000 nm. Other studies [21–25] have also shown new absorption bands to grow at around the same wavelengths upon increase of the doping level of a PAz film. The doping-induced bands start to grow when 0.8 V has been applied to the PAz film. In the composite layer the doping-induced bands start to grow already at 0.2 V when also a Faradaic current starts to be visible in the CV (see Fig. 4a). This is an evidence on that the composite becomes conductive at lower potentials compared to pure PAz.

4 Conclusions

An OAz-TiO₂ composite layer was formed by electrochemical polymerization of Az in TBAPF₆-ACN electrolyte solution in nanoporous ITO/TiO₂ electrode. It was shown that a composite layer rather than a bilayer structure was formed. TiO₂ showed some catalytic activity toward oxidation of Az. p-doping of OAz inside the nanoporous TiO₂ layer demonstrated the electron donor property of OAz. The electron accepting power of TiO₂ was observed as a large reduction current in the negative potential scan. It was shown by CV measurements that the donor-acceptor

combination in the OAz-TiO₂ composite layer enhances also the electron accepting property of TiO₂ compared to pure nanoporous TiO₂. The anatase structure of TiO₂ remained unaltered during electropolymerization of Az. FTIR measurements showed that shorter chains were formed in the OAz-TiO₂ composite due to the higher content of monosubstituted Az rings compared to the PAz film. The composite material had a broad absorbance in the UV-vis spectral region, and it becomes conductive at lower potentials compared to pure PAz.

Acknowledgments This study is a part of the Åbo Akademi University, Process Chemistry Centre, appointed to a National Centre of Excellence by the Academy of Finland for 2000–2011. The authors thank Dr. Kaj Fröberg for performing the XRD analyses, and M.Sc. Linus Silvander for taking the SEM micrographs.

References

- Kamat PV (2007) J Phys Chem C 111:2834
- Bouclé J, Ravirajan P, Nelson J (2007) J Mater Chem 17:3141
- Holder E, Tessler N, Rogach L (2008) J Mater Chem 18:1064
- Senadeera R, Fukuri N, Saito Y, Kitamura T, Wada Y, Yanagida S (2005) Chem Commun 2259
- Senadeera GKR, Pathirathne WMTC (2004) Curr Sci 87:339
- Senadeera GKR, Kitamura T, Wada Y, Yanagida S (2005) Sol Energy Mater Sol cells 88:315
- Senadeera GKR, Kitamura T, Wada T, Yanagida S (2006) J Photochem Photobiol A Chem 184:234
- Liu Y, Scully SR, McGehee MD, Liu J, Luscombe CK, Fréchet JMJ, Shaheen SE, Ginley DS (2006) J Phys Chem B 110:3257
- Song MY, Kim JK, Kim K-J, Kim DY (2003) Synth Met 137:1387
- Ravirajan P, Haque SA, Durrant JR, Poplavskyy D, Bradley DDC, Nelson J (2004) J Appl Phys 95:1473
- Itoh E, Takamizawa Y, Miyairi K (2008) Jpn J Appl Phys 47:509
- Salafsky JS (1999) Phys Rev B 59:10885
- Wang L, Ji J-S, Lin Y-J, Rwei S-P (2005) Synth Met 155:677
- Cuentas-Gallegos AK, Rincón ME, Orozco-Gamboa G (2006) Electrochim Acta 51:3794
- Lin Y-J, Wang L, Chiu W-Y (2006) Thin Solid Films 511–512:199
- Wang G, Chen H, Zhang H, Shen Y, Yuan C, Lu Z, Wang G, Yang W (1998) Phys Lett A 237:165
- Ilieva M, Ivanov S, Tsakova V (2008) J Appl Electrochem 38:63
- Grätzel M (2001) Nature 414:338
- Rasmussen SC, Pomerantz M (2007) In: Skotheim TA, Reynolds JR (eds) Handbook of conducting polymers, 3rd edn. CRC Press, Boca Raton Chapter 12
- Nöll G, Lambert C, Lynch M, Porsch M, Daub J (2008) J Phys Chem C 112:2156
- Lete C, Meana Esteban B, Kvarnström C, Razus A, Ivaska A (2007) Electrochim Acta 52:6476
- Hayashi S, Nakajima S, Kaneto K, Yoshino K (1986) Solid State Commun 60:545
- Shim Y-B, Park S-M (1997) J Electrochem Soc 144:3027
- Porsch M, Sigl-Seifert G, Daub J (1997) Adv Mater 9:635
- Nie G, Cai T, Zhang S, Hou J, Xu J, Han X (2007) Mater Lett 61:3079
- Wang F, Lai Y-H, Kocherginsky NM, Kosteski YY (2003) Org Lett 5:995
- Nakatsuji M, Hata Y, Fujihara T, Yamamoto K, Sasaki M, Takekuma H, Yoshihara M, Minematsu T, Takekuma S-I (2004) Tetrahedron 60:5983
- Meana Esteban B, Lete C, Kvarnström C, Ivaska A (2006) J Phys Chem B 110:23343
- Österholm A, Meana Esteban B, Kvarnström C, Ivaska A (2008) J Electroanal Chem 613:160
- Österholm A, Meana-Esteban B, Kvarnström C, Ivaska A (2008) J Phys Chem B 112:6331
- Österholm A, Petri A, Kvarnström C, Ivaska A, Dunsch L (2008) J Phys Chem B 112:14149
- Dias JR (2007) J Phys Org Chem 20:395
- Zhang X-H, Li C, Wang W-B, Cheng X-X, Wang X-S, Zhang B-W (2007) J Mater Chem 17:642
- Pagba C, Zordan G, Galloppini E, Piatnitski EL, Hore S, Deshayes K, Piotrowiak P (2004) J Am Chem Soc 126:9888
- Tourillon G, Garnier F (1982) J Electroanal Chem 135:173
- Iwasaki K, Tatematsu H, Taneda Y, Matsumoto K, Hino S (1995) Synth Met 69:543
- Cui X, Jiang Z (2003) J Chin Chem Soc 50:1003
- Berger T, Lana-Vilarreal T, Monllor-Satoca D, Gómez R (2007) J Phys Chem C 111:9936
- de la Garza L, Saponjic ZV, Dimitrijevic NM, Thurnauer MC, Rajh T (2006) J Phys Chem B 110:680
- Wu S, Han H, Tai Q, Zhang J, Xu S, Zhou C, Yang Y, Hu H, Chen B, Zhao X-Z (2008) J Power Sources 182:119
- Wang H, He J, Boschloo G, Lindström H, Hagfeldt A, Lindqvist S-E (2001) J Phys Chem B 105:2529
- Cao F, Oskam G, Searson PC, Stipkala JM, Heimer TA, Farzad F, Meyer GJ (1995) J Phys Chem 99:11974
- Liu Y-C, Huang J-M, Tsai C-E, Chuang TC, Wang C-C (2004) Chem Phys Lett 387:155
- Latonen R-M, Meana Esteban B, Kvarnström C, Ivaska A (2009) J Appl Electrochem 39:653
- Gottesfeld S, Redondo A, Rubinstein I, Feldberg SW (1989) J Electroanal Chem 265:15
- Crooks RM, Chyan OMR, Wrighton MS (1989) Chem Mater 1:2
- Zotti G, Schiavon G, Zecchin S (1995) Synth Met 72:275
- Levi MD, Gofer Y, Aurbach D, Lapkowski M, Vieil E, Serose J (2000) J Electrochem Soc 147:1096
- Seshadri V, Wu L, Sotzing GA (2003) Langmuir 19:9479
- Österholm A, Kvarnström C, Ivaska A (manuscript)
- Baia L, Peter A, Cosoveanu V, Indrea E, Baia M, Popp J, Danciu V (2006) Thin Solid Films 511–512:512
- Bian C, Yu Y, Xue G (2007) J Appl Polym Sci 104:21
- Song MY, Kim DK, Ihn KJ, Jo SM, Kim DY (2005) Synth Met 153:77
- Socrates G (2001) Infrared and Raman characteristic group frequencies, tables and charts, 3rd edn. Wiley, Chichester
- Nyquist RA (2001) Interpreting Infrared, Raman, and Nuclear Magnetic Resonance Spectra, vol 2. Academic Press, San Diego
- Wang F, Lai Y-H, Han M-Y (2004) Macromolecules 37:3222
- Zagórska M, Proń A, Lefrant S (1997) In: Nalwa HS (ed) Handbook of organic conductive molecules and polymers, vol 3. Wiley, Chichester